Textured domains on tense surfaces and membranes: Effect of tilt and chirality

R. C. Sarasij,[1] Pragya Srivastava,[1] and Madan Rao[1,2,*]
[1]*Raman Research Institute, C. V. Raman Avenue, Bangalore 560080, India*
[2]*National Centre for Biological Sciences (TIFR), Bellary Road, Bangalore 560065, India*
(Received 19 January 2012; published 26 April 2012)

We study the shape and texture of finite domains comprising chiral or achiral molecules carrying tilt, embedded in a two-dimensional surface or membrane, using a combination of simulations and *exact* variational calculations. We find a variety of shapes and textures including rectangular-shaped domains and a spontaneously broken chiral texture, when the molecules are achiral. We show that chiral tilt domains nucleating in a region of two-phase coexistence *repel* each other, thereby preventing coalescence and further growth. Our work principally addresses observations of domains in multicomponent giant unilamellar vesicles. It may also be relevant in the study of domains in phospholipid monolayers, nucleating domains of Sm-C* in Sm-A films, and chiral emulsions in Sm-A films, in situations where we can ignore dipolar interactions.

DOI: 10.1103/PhysRevE.85.041920 PACS number(s): 87.16.dt

I. INTRODUCTION

Shapes and textures of finite-size domains embedded in surfaces or membranes are governed by an interplay among elasticity, boundary effects, and defect configurations. A particularly interesting realization of distinctive shapes and patterns arises in the context of multicomponent lipid mixtures in freely suspended monolayers [1] and bilayers (e.g., giant unilamellar vesicles; GUVs) [2–9], taken as model systems for the hypothesized lipid-based "rafts" [10,11] on the surface of living cells. Tense GUVs made from binary or ternary lipid mixtures, such as DOPC:DPPC, often exhibit coexistence of liquid disordered (L_d) and gel phases (or even a liquid ordered phase; L_o) over a range of temperatures and compositions, characterized by highly anisotropic domains (and even rosette patterns) of the gel. Such anisotropic patterning naturally arises from the existence of some form of in-plane order, such as tilt order [12].

Our purpose is to provide a detailed analytical and numerical study of the shapes and textures of finite-size domains in two dimensions when the constituent molecules (or molecular aggregates) are both chiral [13,14] and possess a tilt [13,15,16]. While dipolar interactions can often play a crucial role [17,18], we ignore them in this paper; even with this simplification, we discover a complex phase diagram, with a variety of novel phases and symmetry breakings. Both domain shape and tilt texture may be explored by fluorescence microscopy: the former using partitioning of fluorescent probes [5–9]; the latter, by analyzing changes in generalized polarization from probes such as Laurdan [19].

As long as the effects of dipolar interactions can be ignored, our work may have broader implications for a wide variety of soft materials such as (i) domains in freely suspended phospholipid monolayers in an air-water interface [20–24], (ii) nucleation of Sm-C* domains in freely suspended Sm-A films at the A-C* transition [25], (iii) droplets of a suspension of ferromagnetic particles in a liquid film [26], and (iv) emulsion of chiral nematogens in a liquid film [27]. A variety of techniques such as fluorescence confocal polarization microscopy, atomic force microscopy, Brewster-angle microscopy and Bitter microscopy (in the case of ferrofluids) has been used to detect domain shapes and textures on two-dimensional (2D) substrates.

Over the years, there has been a substantial amount of experimental and theoretical work on domain shapes in two dimensions, incorporating the effects of a variety of in-plane orders such as tilt [28] and hexatic [29,30]. However, most theoretical work has been restricted to the case where the constituent molecules are achiral. Here, we systematically study the effects of chirality on the shape and texture of tilt domains using a simplified model Hamiltonian. The competition among bulk orientational order, chirality, and anisotropic line tension from the boundary gives rise to a variety of shapes and textures. Even in the achiral limit we point out several new phases missing in earlier analyses, such as *annular* and *rectangular* domains, which we establish using an " exact" variational approach (whose meaning is made clear later). Unlike previous studies, our variational calculation allows the topology of the domain (connectedness) and the shape of the boundary to vary. Our method of analysis takes off from and extends the elegant treatment in Ref. [28].

In the next section, we discuss the various contributions to the domain energy containing chiral molecules with an orientational field. We arrive at an effective continuum Hamiltonian (Sec. II A) describing the shape and texture of this finite, 2D domain. We next discuss (Sec. III) the optimum shape and orientational ordering within the finite patch of fixed area. The main results of this paper are as follows. (i) We obtain an " exact" phase diagram in the achiral limit when the boundary of the domain is circular (Sec. III A), with a variety of optimal textures such as virtual boojum, defect, achiral annular, and a spontaneously broken chiral annular phase. (ii) We study smooth perturbations of the boundary and determine the regime of instability of the circular domain (Sec. III B) and the nature of the resulting equilibrium phase. We find that the annular phases are no longer minimum energy configurations. Typical domain shapes are thin and elongated, best described as rectangular. (iii) Turning on bulk chirality gives rise to a spiral defect phase and a novel chiral tweed phase (Sec. III C). (iv) Chirality may even induce a large enough domain to split into multiple domains; we determine the conditions under

*rao.madan@gmail.com

which such multiple domains are obtained (Sec. IV). This suggests that tilt domains, nucleated following a quench across a phase boundary in a multicomponent system, would repel each other, preventing coalescence and subsequent growth. We end with a short discussion (Sec. V).

II. ORDER PARAMETER AND EFFECTIVE HAMILTONIAN

What is the equilibrium texture of a collection of chiral molecules described by an orientational field, uniformly spread over a finite domain of fixed area A embedded in a 2D flat substrate, such as a tense GUV? We show that the interplay between orientational ordering and domain shape gives rise to a variety of novel phases and shape transitions. We first discuss the nature of the order parameter and the dominant contributions to the energy of the domain.

The orientation of a rigid molecule may be described by a polar vector which takes values in S^2 (Heisenberg spin) or a director which takes values in the projective space $RP^2 \equiv S^2/Z_2$ [31]. However energetic considerations, e.g., in the case of membranes, a combination of van der Waals and hydrophobic shielding, may constrain (a) the center of mass of the molecules to lie on a 2D, flat surface and (b) the projection of the long axis of the molecule onto the 2D plane to have a fixed magnitude (or small deviations from a fixed value). Thus owing to strong uniaxial anisotropy, the low-energy sector may be described by a 2D polar vector $\mathbf{m}$ (since the 2D surface carries a unique local outward normal) which takes values in S^1, an XY spin. The center-of-mass density $\rho(x,y)$ of the molecules is assumed to be uniformly smeared over the patch of area A. The molecules outside the finite patch are assumed to be either in the isotropic or in the Sm-A (i.e., no tilt) or the liquid-disordered (L_d) phase.

The tilt molecules interact with each other, and with the molecules outside the patch, both sterically (purely repulsive) and via short-range (e.g., van der Waals) attractive interactions. Both these effects contribute to chiral interactions: the former, via the Straley picture of interlocking screws [32]; the latter, via a generalization of the Van der Waals dispersion to chiral molecules [33]. In the continuum limit, these short-range interactions can be written as the usual Frank energy, modified to include the effects of chirality.

In this paper, we ignore the contribution coming from dipolar interactions. In some cases, such as in phospholipid domains on GUVs, this may be justified, since the Frank elastic constants are of order $10k_BT$ (at room temperature), while the dipolar energy per phospholipid is about $0.1k_BT$. In situations where dipolar energy scales are comparable, it is likely to have a major effect on domain shapes and textures, such as, for instance, the formation of string-like aggregates [34].

In our present treatment we assume the surface or membrane to be flat over the scale of the patch; thermal undulations of the surface controlled by surface tension or bending rigidity are assumed to be negligible over this scale. Elsewhere we have discussed the effect of chiral tilt textures on a *flexible membrane*, leading to a novel chirality-induced budding and tubulation [35,36].

A. Tilt texture Hamiltonian

Let us assume that the molecules, now described by a 2D orientational field $\mathbf{m}$, are smeared with a fixed, uniform density over a patch (domain) of area A embedded in a 2D surface, the xy plane. The rest of the surface surrounding the patch is a structureless fluid consisting of molecules different from the constituents of the patch (or else in a different phase). We assume that the patch constituents have come together as a result of *strong* phase segregation. The domain energy can be written in terms of bulk distortions of $\mathbf{m}$ and interfacial (perimeter) distortions, including an orientation-interface coupling.

In our low-energy description, the magnitude of $\mathbf{m}$ is held fixed and normalized to unity (hard-spin model). The resulting domain energy only contains phase distortions of $\mathbf{m} \equiv (\cos\phi, \sin\phi)$. Such a *phase-only* theory is formally ultraviolet divergent and needs to be made finite by a microscopic cutoff length of molecular dimensions. The regime of validity of such phase-only theories is over scales larger than this cutoff length. At these scales, the hard-spin model is equivalent to a soft-spin model, where the magnitude of $\mathbf{m}$ is constrained by means of a potential $V(\mathbf{m}) = u(\mathbf{m}\cdot\mathbf{m} - 1)^2$ to deviate only slightly from its preferred value, for u large and postive.

The form of the bulk distortion energy of $\mathbf{m}$ can be constructed from symmetry arguments. Since tilt is a spatial vector, tilt distortions may be described by a Hamiltonian invariant under 2D spatial rotations $O(2)$. To lowest order, this leads to the usual Frank energy in two dimensions, with two independent contributions: a *splay* distortion $(\nabla\cdot\mathbf{m})^2$ and a *bend* distortion $(\nabla\times\mathbf{m})^2$, where $\nabla \equiv (\partial_x, \partial_y)$. Recall, however, that the molecules are chiral, and so on general symmetry grounds, we should allow for terms which are invariant under improper rotations alone; thus to lowest order this gives rise to a term of the form $(\nabla\cdot\mathbf{m})(\nabla\times\mathbf{m})$ [25]. Note that for a 2D vector field $\mathbf{m}$, $\nabla\times\mathbf{m}$ is a pseudoscalar, not a vector. Viewed as a vector in R^3, the curl $\vec{m}$ is a pseudovector pointing along $\vec{z}$ (we consistently represent 2D vectors by boldface and 3D vectors by an overhead arrow).

The coupling between the tilt and the interface gives rise to boundary terms: if $\mathbf{n}$ is the local unit normal to the boundary aiming into the domain, then there are two possible boundary terms to linear order in $\mathbf{m}$. These are (i) an isotropic line tension proportional to the perimeter and (ii) anchoring terms of the form $(\mathbf{m}\cdot\mathbf{n})$ and $(\mathbf{m}\times\mathbf{n})$, which contribute to an effective anisotropic line tension. One source for this boundary term is that the interface between the tilt and the nontilt components (in the case of chiral emulsions, this coincides with the tilt-solvent interface) prefers a specific alignment of the tilt with the local normal. Alternatively, such boundary contributions may arise from the presence of a bulk spontaneous bend $\nabla\times\mathbf{m}$ and splay $\nabla\cdot\mathbf{m}$, since

$$\int_A \mathrm{div}\,\vec{m} = \oint_C \vec{m}\cdot\vec{n}, \tag{1}$$

$$\int_A \mathrm{curl}\,\vec{m} = \oint_C \vec{m}\times\vec{n}. \tag{2}$$

The spontaneous bend is a chiral contribution; spontaneous splay could arise from specific substrate-tilt coupling or from steric forces arising from a high head-to-tail ratio of the constituent molecules.

Thus our low-energy effective Hamiltonian for the chiral tilt domain in the strong segregation limit is given, to quadratic order in the fields, by $E = E_B + E_C$, where the bulk energy

$$E_B = \int_A \left[\frac{k_1}{2}(\nabla \cdot \mathbf{m})^2 + \frac{k_2}{2}(\nabla \times \mathbf{m})^2 + k_c(\nabla \cdot \mathbf{m})(\nabla \times \mathbf{m}) \right] \delta^2 x, \tag{3}$$

and the interfacial energy

$$E_C = \oint_C dl(\sigma_0 + \sigma_1(\mathbf{m} \cdot \mathbf{n}) + \sigma_2(\mathbf{m} \times \mathbf{n})). \tag{4}$$

The coefficients k_1, k_2, and k_c represent the energies of splay, bend, and chiral distortions of the tilt field. When the coefficients k_1 and k_2 are comparable, the Frank terms resist any deviation of $\mathbf{m}$ from uniformity and hence the $\mathbf{m}$ field would everywhere point in a specific direction. The anisotropic boundary terms, σ_1 (σ_2), however prefer to align $\mathbf{m}$ at the boundary along (or orthogonal to) the local normal. This competition gives rise to a variety of nontrivial textures. The boundary terms may be interpreted as providing an effective anisotropic line tension of the form $\sigma_0 + \sigma_1(\mathbf{m} \cdot \mathbf{n}) + \sigma_2(\mathbf{m} \times \mathbf{n})$. A negative value of this effective line tension would lead to an instability of the circular domain boundary [28]. Nontrivial textures also obtain when the Frank coefficients k_1 and k_2 are appreciably different [37]. We will see that chirality introduces a new twist to the texture phase diagram [35,36].

In this strong segregation limit, molecules are not allowed to exchange across the domain. This imposes a constraint on the allowable configurations explored by the molecules. Thus for fixed "bath" conditions (state of the molecules outside the patch), the configuration of molecules inside the patch can reach equilibrium. The area of the patch and the density of molecules in the patch are fixed over this time scale. In the case of nucleation of the chiral tilt domains (e.g., Sm-C* domains in a freely suspended Sm-A film or tilt domains of chiral lipids in a mono- or bilayer), slow domain growth justifies the use of quasiequilibrium ideas. For a dilute emulsion, the area of the domain is fixed at time scales smaller than the domain coalescence times; thus the shape and texture of the domain will be such as to minimize the free-energy subject to the constraint of constant area.

Our aim, then, is to find that optimal conformation: in general, a difficult calculational task. We will see that given the energy scales in the problem (Sec. V), we may ignore the effects of thermal fluctuations on the shape and texture of the domain. Thus, the Frank constants k_1,k_2 are $\sim 10 k_B T$, while the interfacial energy of a domain of radius $10\,\mu$m is an order larger. Hence a mean-field minimization of the above free-energy functional will suffice. Estimates of the line tensions obtained from studies of shape and texture changes of tilt domains in Langmuir monolayers using Brewster angle microscopy [23] and shapes of lipid domains in GUVs using fluorescence microscopy [9] give $\sigma_0 \approx 0.4 k_B T$/nm for the isotropic and $\sigma_1 \approx 0.36 \times 10^{-3} k_B T$/nm for the anisotropic line tensions, respectively.

III. MEAN-FIELD PHASE DIAGRAM

We perform this constraint minimization of the free energy using a variational approach, where we vary both the texture and the domain shape while keeping the area constant. Our constrained variational ansatz also accounts for the possibility that the domain may not be simply connected, however, we will not allow the domain to break up (domain splitting will be treated in Sec. IV). Our variational guesses are supported by computer simulations, i.e., Monte Carlo simulations with simulated annealing to avoid getting stuck in local minima. It is in this sense that our variational calculation for the mean-field phase diagram is " exact" (made more explicit in Sec. III A). We have also explicitly checked that the effect of including higher-order (symmetry allowed) terms in the Hamiltonian is small and does not affect the phase diagram.

We henceforth set $k_1 = 1$ as our unit of energy and $R = 1$, associated with the domain size $R = \sqrt{A/\pi}$, as our unit of length. Some experimental situations are more conveniently analyzed by fixing $\sigma_0 = 1$ as the unit of length and determining the phase structure in the (R,σ_1) plane. We discuss both these ensembles.

Given the total energy functional, we obtain the optimal conformation of the domain shape and texture that minimizes this energy, subject to two constraints. One is that the orientation $\mathbf{m}$ is a unit vector: this may be ensured by either a "hard-spin" version of the model (where we explicitly set $|\mathbf{m}| = 1$, by suitable parametrization) or a soft-spin potential of the form $V(\mathbf{m}) = -\alpha(\mathbf{m} \cdot \mathbf{m}) + \beta(\mathbf{m} \cdot \mathbf{m})^2$ or $V(\mathbf{m}) = u(\mathbf{m} \cdot \mathbf{m} - 1)^2$, which makes deviations of $|\mathbf{m}|$ from unity hard to obtain.

A. Achiral domain

We first turn off the effects of bulk chirality ($k_c = 0$) but retain the anisotropic boundary term. In most of our work we take $k_2 = k_1 = K$ (the one-coupling-constant approximation); toward the end we comment on the distinct features when $k_1 \neq k_2$.

In terms of the phase angle ϕ, where $\mathbf{m} \equiv (\cos\phi, \sin\phi)$, the free-energy functional simplifies to

$$E = \frac{K}{2} \int_A (\nabla\phi)^2 + \oint dl(\sigma_0 + \sigma_1 \cos(\psi - \phi) + \sigma_2 \sin(\psi - \phi)), \tag{5}$$

where we have written the normal $\mathbf{n} \equiv (\cos\psi, \sin\psi)$ in polar coordinates. Variation of the above Hamiltonian gives the *bulk* Euler-Lagrange equation, $\nabla^2\phi = 0$ (Laplace) and nontrivial boundary equations which have to be simultaneously satisfied. Instead of asking for solutions of the combined bulk + boundary equations, we determine the global minimum free-energy configuration variationally: this has the advantage of obtaining *boundary minima*, minimum energy configurations that may not be solutions of the Euler-Lagrange equations.

Without loss of generality, we may work with a simplified free-energy functional: as argued by previous authors [25,28], a global rotation of $\mathbf{m}$ by $\phi' = \phi - \tan^{-1}(\sigma_2/\sigma_1) - \pi/2$, without rotating the boundary contour, transforms the

free-energy functional to a new functional,

$$E = \frac{K}{2}\int_A (\nabla\phi)^2 + \oint dl(\sigma_0 + \sigma\cos(\phi - \psi)), \qquad (6)$$

where $\sigma = \sqrt{\sigma_1^2 + \sigma_2^2}$ is the single redefined anisotropic boundary coefficient. Configurations which minimize the free energy, (5), with parameters $(K,\sigma_0,\sigma_1,\sigma_2)$ can be obtained from configurations which minimize the free energy, (6), with parameters (K,σ_0,σ) via the global transformation defined above. Thus in this equal-constants, achiral regime, it suffices to work out the phase diagram in the (σ_0,σ) plane using the free energy, (6); the phase diagram for arbitrary values of σ_1, σ_2 can then be reconstructed. This simplification does not occur when the bulk chiral term is present. Note that by making a global rotation, it is possible to entirely eliminate the contribution from the boundary chiral term $\nabla \times \mathbf{m}$. This implies that the domain shapes will always be achiral [28]. Now set $R = 1$, as our unit of length. We first discuss the limit of large σ_0, when the domains are forced to be circular (we discuss the limit of stability of a circular domain in Sec. IV). The extreme limit, $\sigma_0 \to \infty$, might be experimentally arranged by smearing a thin film of Sm-C* over a hole made in a solid substrate. Clearly, in the absence of any anisotropic line tension, $\sigma = 0$, the lines of **m** describing the optimal texture are a (parallel) set of straight lines pointing in *any* direction. This configuration is invariant under arbitrary translations and rotations of the boundary circle with respect to the lines of **m**. An infinitesimal (positive) σ forces the lines of **m** to curve slightly (at the cost of Frank energy) to meet the circular domain boundary at a desired angle (Fig. 1). From the axial symmetry of the solution, it is clear that this configuration is associated with a +2 virtual defect, situated *outside* the domain, called a *virtual boojum* [25]. Note that this configuration is infinitely degenerate. To calculate the energy we need to parametrize the virtual boojum configuration, where the center of the circular domain is a distance, a, away from the core of a virtual defect of strength N. Placing the origin of polar coordinates (r,θ) at the core of the boojum, we can describe the texture $\mathbf{m} \equiv (\cos\phi, \sin\phi)$ by the equation

$$\phi = N\theta + c_1 r\sin\theta + c_2 r^2\sin 2\theta + c_3 r^3\sin 3\theta + \cdots. \qquad (7)$$

The first term is the singular part representing the boojum; subsequent terms represent the most general smooth solution of Laplace's equation with the desired symmetry. The energy E is minimized with respect to the variational parameters $(N,a,\{c_n\})$ for fixed (σ_0,σ). Consistent with our symmetry arguments, we explicitly find that the optimal value of N is

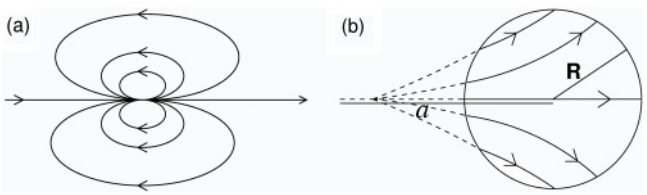

FIG. 1. Effect of anisotropic line tension on the texture of an achiral circular domain: (a) a boojum of charge 2; (b) texture of a domain of radius R whose center is at a distance a from the core of the boojum. Arrows give the local direction of **m**.

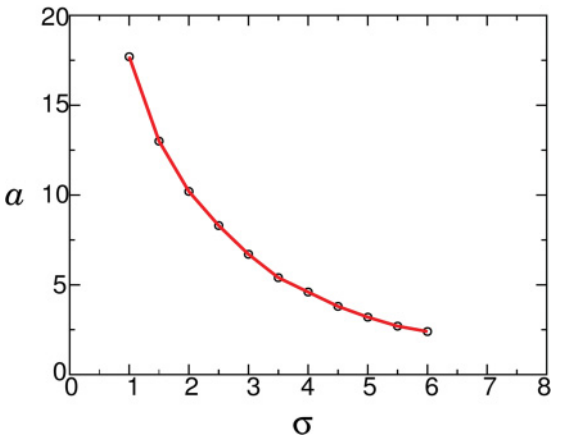

FIG. 2. (Color online) Variation of a, the distance of the virtual boojum from the center of the domain, as a function of the anisotropic line tension σ: note that the penetration of the boojum core into the domain is pre-empted by the annular phase. We have taken $\sigma_0 = 1$ for convenience.

exactly 2 and independent of a. In principle, of course, we can take as many variational parameters $\{c_n\}$ as we desire; however, in drawing the phase diagram we have parametrized the texture by a and c_1 alone; inclusion of higher order c_n lowers the energy by 1% at most. The form of the variational energy for $\phi = 2\theta$ is given by [28]

$$E(a) = -2\pi K\ln\left[1 - \left(\frac{R}{a}\right)^2\right] - 2\pi\frac{\sigma R^2}{a} + 2\pi\sigma_0 R, \qquad (8)$$

which is to be minimized with respect to a. The minimization with respect to the whole set of parameters $(a,\{c_n\})$, however, is best carried out numerically. Upon variation, we find that an increase in the anisotropic line tension σ leads to an increase in c_1, pushing the core of the virtual defect toward the domain center. Experimental characterization of this texture in the context of Langmuir monolayers at the air-water interface [23,24] agrees with our analysis above. This movement of the core continues till $a = 1.7$, beyond which there is a discontinuous transition to the annular phase (Fig. 2). Note that the boojum is always virtual; the core never penetrates the domain, since it is pre-empted by the annular phase. Reference [28] misses this feature, since their variational shapes do not include such multiply connected topologies.

The *achiral annular* phase can be parametrized by inner and outer radii r_1 and r_2, respectively. At the outer rim of the annulus, **m** is directed radially outward, while at the inner boundary, **m** is inclined at an angle α to the local normal **n**. With the origin of polar coordinates at the center of the annulus, the texture may be described by

$$\phi = \theta - \alpha\frac{r_2 - r}{r_2 - r_1}, \qquad (9)$$

where r_1, α are variational parameters (r_2 may be obtained from the constant area constraint). With this parametrization, the energy of this configuration is given by

$$E(r_1,\alpha) = \pi K\left[\frac{\alpha^2}{2}\left(\frac{r_2 + r_1}{r_2 - r_1}\right) + \ln\frac{r_2}{r_1}\right] - 2\pi\sigma(r_2 - r_1\cos\alpha) + 2\pi\sigma_0(r_1 + r_2), \qquad (10)$$

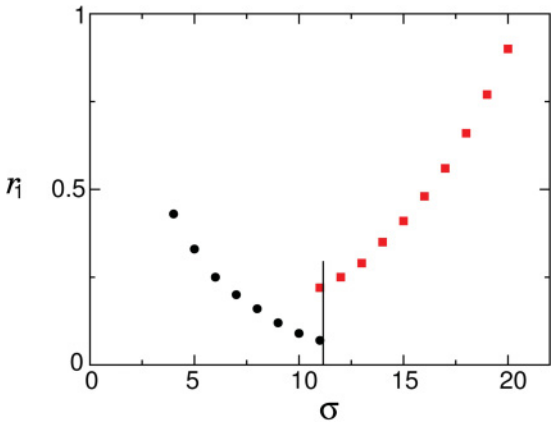

FIG. 3. (Color online) The inner radius r_1 of the annular domain decreases (increases) with σ in the achiral (chiral) phases [represented by circles (squares)]. We have taken $\sigma_0 = 1$ for convenience.

where $r_2^2 - r_1^2 = R^2$. The inner radius r_1 monotonically decreases as we increase σ (Fig. 3) such that $\mathbf{m}$ always points radially outward ($\alpha = 0$) at every point of the domain. With increasing σ, we cross a first-order phase boundary (Fig. 4) into a new annular phase with a chiral texture.

The *chiral annular* phase is obtained when the angle α jumps to a value greater than $\pi/2$ at both the inner and the outer boundaries. The bulk texture is chiral and is a true symmetry-broken configuration (recall that there is no bulk chiral interaction) with the pseudoscalar order parameter

$$C = \frac{1}{R}\int d^2x\,(\nabla \times \mathbf{m}) \neq \mathbf{0}. \tag{11}$$

This chiral phase is doubly degenerate and can spontaneously acquire either sign; the anisotropic tension σ behaves as a *surface* field conjugate to this Ising-like chiral order parameter.

Note that the "core" of these annuli must consist of molecules without tilt; our assumption in minimizing the energy has been that the two species of molecules are free to diffuse across the domain of fixed area A. If for some reason

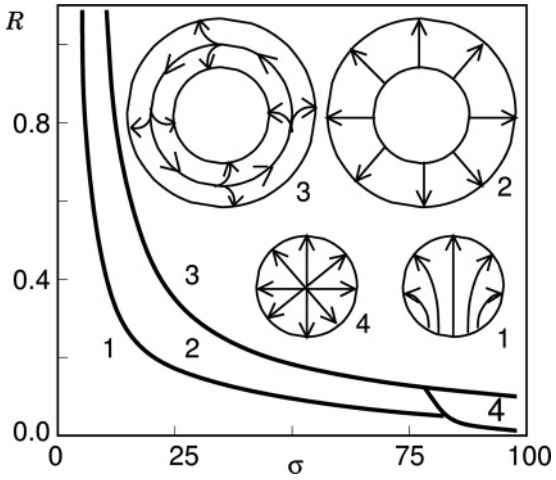

FIG. 4. Phases of the tilt texture domain with a circular periphery: (1) virtual boojum; (2) achiral annular; (3) chiral annular; (4) hedgehog with $\epsilon_c = 0$. Arrows indicate the direction of the $\mathbf{m}$ field.

the diffusion of the nontilt molecules from outside the patch to the core of the annulus is hindered, then the appearance of such a phase would be kinetically blocked. In this case, the virtual boojum will penetrate the domain and would lead ultimately to the hedgehog configuration (as in Ref. [28]).

The *hedgehog* phase has a defect at the domain center and a texture described by $\phi = \theta$ (when the origin is at the domain center). The energy includes a core contribution ϵ_c of the defect of *microscopic* size r_c ($r_c \ll R$),

$$E_{\text{hedge}} = \pi K \ln\frac{R}{r_c} - 2\pi R(\sigma - \sigma_0) + \epsilon_c. \tag{12}$$

The phase diagram in the (R,σ) plane is shown in Fig. 4. The transitions between these phases are discontinuous, as indicated by the change in slope of the energy branches as a function of σ. As discussed earlier, in some experimental situations it is more useful to study the phase diagram in the (R,σ) plane; thus we set $\sigma_0 = 1$ to obtain a unit of length. Assuming that the domain is still circular, the phase diagram shows the discontinuous transitions, which weaken (i.e., the jump in the appropriate order parameter decreases) as the domain size R shrinks.

This analysis suffices to reconstruct the entire phase diagram in the (σ_1,σ_2) plane by global rotation of the optimal textures obtained above. For instance, the virtual boojum texture reported in Ref. [28] can be obtained from a global rotation of the texture in Fig. 1. Likewise, the *vortex* phase can be obtained by globally rotating the hedgehog texture by an angle $\pi/2$. The vortex texture spontaneously breaks chiral symmetry. Other nontrivial phases may be obtained by global rotations of the texture in the annular phases.

Finally, we mention in passing the case where $k_1 \neq k_2$, which was the subject of study in Ref. [37]. The difference in the splay and bend energies implies that the hedgehog and vortex defects are no longer degenerate. If $\Delta K = (k_1 - k_2)/k_1$, then as ΔK goes from large negative to large positive values, the texture goes from a hedgehog to a vortex via a spiral defect phase.

B. Noncircular achiral domain

For smaller values of σ_0/σ_1, the domain is no longer circular; as shown in Refs. [28,38], deviations from circularity arise when the effective line tension $\sigma_0 + \sigma_1(\mathbf{m}\cdot\mathbf{n}) + \sigma_2(\mathbf{m}\times\mathbf{n}) < \mathbf{0}$. We summarize their results, based on linear stability analysis.

Parametrize the boundary by smooth deformations of a circle, $r(\theta)$, where we have temporarily shifted the origin from the core of the boojum by a distance a to the center of the domain, i.e., the center of the circle of radius r_0, and $0 < \theta < 2\pi$ is the angle to the polar axis,

$$r(\theta) = r_0\left(1 + \sum_{n=1}^{\infty}\alpha_n \cos n\theta\right). \tag{13}$$

Such a parametrization only includes shapes with no overhangs; i.e., the coordinate $r(\theta)$ is a single-valued function of θ. Further, the parametrization is smooth and so does not include shapes with cusps, as in Refs. [24,38]. Since the area of the

domain has to be A, we must have

$$\pi r_0^2 \left(1 + \frac{1}{2}\sum_{n=1}^{\infty} \alpha_n^2\right) = A = \pi r^2. \tag{14}$$

Perturbative analysis [28] of the domain boundary about the circle *and* the texture about the optimal texture (virtual boojum, annuli or hedgehog), as carried out in Ref. [28] for the virtual boojum, indicates that the circle is unstable to the $n = 2$ mode when $\sigma > \sigma_0$, below a critical value of $K/\sigma R$.

We complement the linear stability analysis by a variational calculation. The reason we do this is because (a) linear stability analysis typically underestimates phase boundaries and (b) linear stability analysis does not give the (new) stable configuration in the regime of instability of the circle. To address these issues, we parametrize both the boundary and the texture and determine the lowest energy configurations of the texture and the domain shape using a variational scheme.

Again, we set $K = \sigma_0 = 1$ to fix the units of length and energy. We now minimize the energy as a function of variational parameters $\{N, a, \{c_n\}, \{\alpha_n\}\}$ for a given value of R and σ. The optimal value of N is, as before, $N = 2$. We also find that including terms in the texture with coefficients $\{c_{n>1}\}$ reduces the minimum value of E by at most 1%. So we parametrize the texture in the simpler form

$$\phi = 2\theta + c_1 y, \tag{15}$$

where y is the distance of any point from the axis of the domain. As σ is increased from 0, the core of the boojum approaches the center of the domain but the domain remains almost circular.

As σ is raised beyond a threshold σ^*, the core begins to recede from the center and the domain bulges out at the equator (Fig. 5) and flattens near the poles. Indeed we find that the texture throughout the (R,σ) plane is either a virtual boojum or a hedgehog defect. For large values of σ, but still in the boojum phase, it is a good approximation to set $\phi = c_1 y$ and take the domain to be a rectangle bracketed at the equator by two semicircular caps (Fig. 5). When the defect is within the domain, the texture is a hedgehog; we leave the study of the corresponding domain shapes for later.

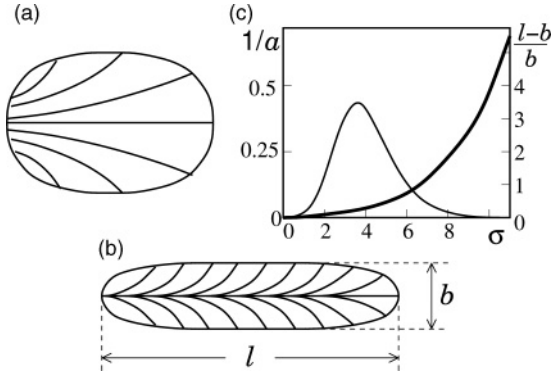

FIG. 5. Stretching action of strong anisotropic line tension: domain conformation for (a) $\sigma = 6.5$ and (b) $\sigma = 9.5$. (c) Variation of $1/a$ (thin line) and the prolateness $(l - b)/b$ with σ for a domain of effective radius $R = 1$.

Such rectangular domains have been observed on GUVs consisting of a binary lipid mixture, a saturated component (e.g., DPPC) and an unsaturated component (e.g., DOPC), at temperatures below the gel transition of the saturated lipid (e.g., 42 °C for DPPC). Following a temperature quench, domains of the saturated lipid, observed using fluorescence microscopy, were found to nucleate in the background of the unsaturated lipid and grow as rectangular domains. We suggest that the tilt of DPPC in the gel phase gives rise to an anisotropic line tension, accounting for the shape of these domains, consistent with our analysis.

C. Chiral domain

We now turn to a description of the phases with nonzero bulk chirality k_c. In this case, both the texture and the shape of the boundary may assume chiral shapes. For the moment, however, let us assume that the boundary of the patch is circular. As before, we set $k_1 = k_2 = 1$ and $\sigma_0 = 1$. Further, without loss of generality, we take $k_c > 0$. To highlight the effects of bulk chirality, we have set the anisotropic line tension $\sigma = 0$. It will be clear that the effects of bulk chirality dominate the nature of the texture.

Let us rewrite the Frank expression as

$$E = 2\pi R + \int_A \frac{1}{2}(\operatorname{div}\mathbf{m} + \operatorname{curl}\mathbf{m})^2 + (k_c - 1)(\operatorname{div}\mathbf{m})(\operatorname{curl}\mathbf{m}). \tag{16}$$

It is clear, and we have checked this explicitly, that for a low enough bulk chirality, $|k_c| < 1$, the *uniform* phase, with a circular domain and uniform $\mathbf{m}$, is the lowest energy state. Indeed, had we included the anisotropic line tension, we would have seen that the optimal achiral domains described in Fig. 4 would be the lowest energy configurations for small enough $|k_c|$.

As seen in Eq. (16), increasing the magnitude of k_c, makes the optimal texture more wound up: the texture prefers to have a very high curl and a divergence equal and opposite to the curl. The optimal texture is neither a pure divergence nor purely rotational, but an (Archimedes) spiral with an angle of opening $\alpha = \pi/4$ with respect to the local radial (Fig. 6).

In polar coordinates, with the origin at the center of the circular domain, the *spiral hedgehog* is described by an $\mathbf{m}$ with constant radial and tangential components everywhere, $m_r = \cos\alpha$ and $m_\theta = \sin\alpha$ $(m_r^2 + m_\phi^2 = 1)$. Using

$$\operatorname{div}\mathbf{m} = \frac{m_r}{r}, \tag{17}$$

$$\operatorname{curl}\mathbf{m} = \frac{m_\phi}{r}, \tag{18}$$

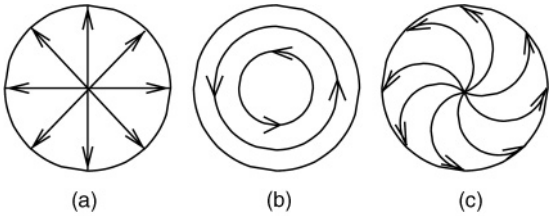

FIG. 6. (a) Pure divergence. (b) Pure rotational. (c) Spiral defect.

we may compute the energy of this spiral configuration,

$$E = 2\pi(r_c + R) - \frac{1}{2}(k_c \sin 2\alpha - 1)\ln\frac{R}{r_c} + \epsilon_c, \quad (19)$$

where r_c is the radius and ϵ_c is the energy of the defect core. The optimum value of α is $\pi/4$ when $|k_c| > 1$, making $m_r = 1/\sqrt{2}, m_\phi = -1/\sqrt{2}$. The spiral hedgehog phase clearly gives a nonzero value for the chiral order parameter C, Eq. (11).

We see that the effect of the k_c term is felt most strongly at the core of the spiral defect, falling off inversely as the square of the distance from the core. Can we find a texture whose chiral strength is large not just at one point but over the entire domain ? If so, this would surely be a candidate for the optimal texture.

To answer this question, we have carried out a Monte Carlo simulation of 3055 particles carrying O(2) spins on a triangular lattice with a Hamiltonian obtained by discretizing E. In order to search for the lowest energy configuration, we had to resort to simulated annealing from $(k_B T)^{-1} = 0.1 \to 300$ starting from a variety of initial conditions. The energy functional is augmented by a higher order term $\gamma\,((\mathrm{div}\,\mathbf{m})^4 + (\mathrm{curl}\,\mathbf{m})^4)$ to provide a cutoff to the spatial variations of $\mathbf{m}$. Figure 7 shows the optimal texture obtained for $\sigma = 0$ and $k_c = 12.75$: the texture is best described as a *chiral tweed* with a stripe size $l^* = 0.01$.

This texture may be easily parametrized variationally. First, place the origin of coordinates on the boundary of the domain with the x axis along a diameter and parametrize the texture by

$$m_x = \left|\cos\frac{x}{l}\right|, \quad m_y = -\left|\sin\frac{x}{l}\right|. \quad (20)$$

The texture consists of stripes of width πl parallel to the y axis. This parametrization is shown in Fig. 7 for comparison with the optimal texture obtained in the simulation. This texture confers a net chiral strength to the domain: $(\nabla\cdot\mathbf{m})(\nabla\times\mathbf{m})$ has the same sign everywhere, although the sign of individual terms, $\nabla\cdot\mathbf{m}$ and $\nabla\times\mathbf{m}$, varies from one stripe to the next. The energy of the chiral tweed domain is

$$E = 2\pi R - \frac{k_c}{2l^2}\int_0^{2R} dx\sqrt{2xR - x^2}\left|\sin\frac{2x}{l}\right| + \frac{\pi R^2}{2l^2}. \quad (21)$$

The variational parameter l approaches 0 to minimize this energy: higher order derivative terms in the Hamiltonian,

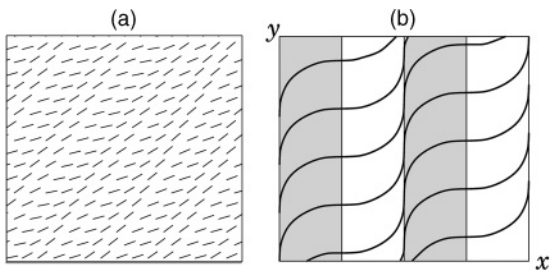

FIG. 7. (a) Closeup of the chiral tweed texture generated by a Monte Carlo simulation, and (b) its continuum representation by a mathematical formula. In the shaded (white) portions, div $\mathbf{m}$ is positive (negative) and curl $\mathbf{m}$ is negative (positive). This shows the texture within a unit cell; the pattern repeats periodically to form the tweed phase.

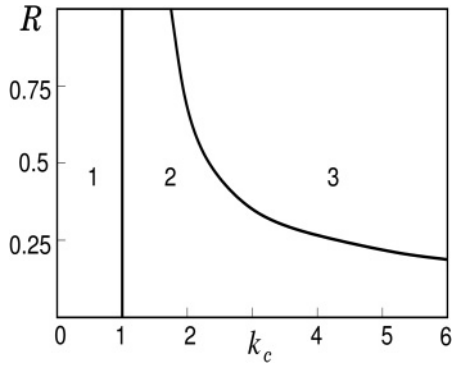

FIG. 8. (a) Phases of the tilt texture domain with bulk chirality and $\sigma = 0$: (1) uniform phase; (2) spiral defect (where we have taken $\epsilon_c = 0$ and $r_c = 0.005$); (3) chiral tweed (stripe width $l^* = 0.01$).

such as $\gamma\,((\mathrm{div}\,\mathbf{m})^4 + (\mathrm{curl}\,\mathbf{m})^4)$, would, however, cut off this monotonic decrease at some scale l^*. Note that the energy decreases rapidly as k_c increases (Fig. 9). The phase diagram of this chiral domain is given in Fig. 8, together with a demonstration of discontinuous transitions as shown by the crossing of the energy branches (Fig. 9).

IV. DOMAIN SPLITTING

So far our restriction to the strong segregation limit has also assumed that the planar domain of area A does not break up. If the chiral strength is large enough, $k_c \gg 1$, the texture might prefer to maximize the number of spiral defect points. This could induce domain splitting. To study the conditions under which such breakup is favorable, we calculate the energy of n circular domains of equal area, each bearing the same spiral texture, and compare it to that of a single circular domain with the same total area and texture. The total energy of this configuration is

$$E^{(n)} = 2\pi\sigma_0\sqrt{n}R - n\pi(k_c - 1)\ln\frac{R/\sqrt{n}}{r_c} + n\epsilon_c. \quad (22)$$

For small values of A, a single domain $E^{(1)}$ has the least energy. As A increases, $E^{(2)}$ becomes smaller than $E^{(1)}$: chirality in the bulk wins over interfacial energy (Fig. 10). As A increases further, multidomain splitting is favored (Fig. 10).

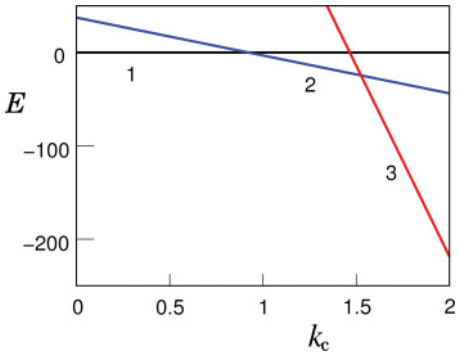

FIG. 9. (Color online) Variation of the energy branches of the (1) uniform, (2) spiral hedgehog, and (3) tweed phases as a function of k_c at $R = 1$, indicating discontinuous transitions. Note that the energy decreases rapidly in phase 3 as k_c increases.

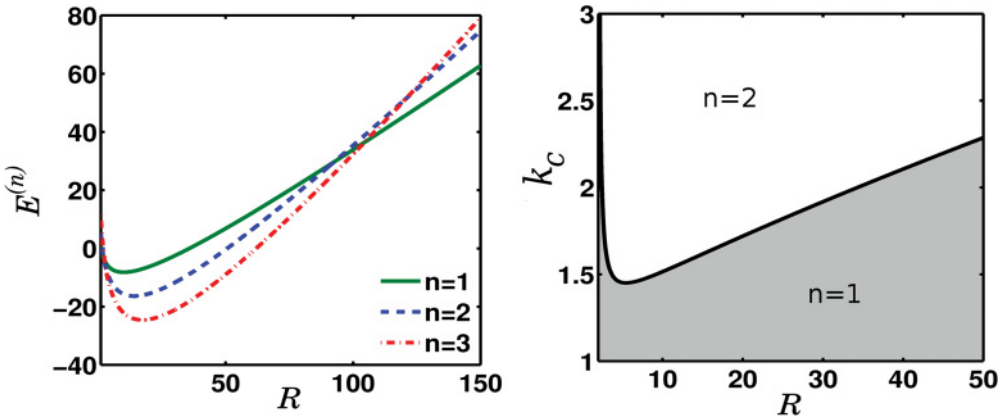

FIG. 10. (Color online) Energy $E^{(n)}$ of a domain split into n equal parts, keeping the total area, $A = \pi R^2$, fixed (R in units of the core radius, r_c). Here we show the $n = 1,2,3$ branches: the domain prefers to split in two for a range of R values ($\sigma_0 r_c = 0.1$, $\epsilon_c = 0$, $k_c = 3$). (b) Phase diagram of k_c versus R (in units of r_c) shows a regime where a single domain ($n = 1$) splits into two domains ($n = 2$).

At even higher values of A, however, domain splitting is prohibited by a large interfacial energy cost; thus there is a window of areas for which chirality induces domain split-up. This tendency to split holds when k_c is large enough; for a fixed value of $\sigma_0 r_c$, there is a critical k_c beyond which chirality-induced splitting would manifest. This splitting phase diagram is shown in Fig. 11. Increasing the value of $\sigma_0 r_c$ increases the value of k_c at which the domain splitting transition takes place.

This chirality-induced splitting has implications in the nucleation and growth of tilt-ordered domains in a fluid substrate, as in binary lipid mixtures, where one of the components has a tilt and is chiral, or in the nucleation of Sm-C* domains in a Sm-A film (since the SmA-SmC* transition can be first order [39]). For instance, consider a GUV composed of a binary lipid mixture of a saturated (minority component) and an unsaturated lipid species, quenched below the gel transition of the saturated lipid. Domains of the gel phase spontaneously nucleate in the liquid-disordered phase. Growth initially occurs via coarsening; as the domains get larger, they undergo random Brownian diffusion on the surface of the GUV, coalescing when two domains encounter each other. If, however, the molecules in the gel phase have a tilt and chirality, then coalescence of large enough domains (determined by the value of k_c; Fig. 11) could be prevented by the above mechanism, leading to a suppression of further growth. A similar feature should be observed in the nucleation and growth of Sm-C* domains in a Sm-A film.

V. DISCUSSION

In this paper we have discussed the equilibrium shapes and textures of a single domain consisting of molecules endowed with a tilt embedded on a rigid surface, in situations where dipolar interactions are unimportant. In addition to having a tilt, the molecules constituting the domain may be chiral. The interplay among tilt, chirality, and boundary effects gives rise to a rich variety of shapes and textures separated by discontinuous transitions. Our results are obtained by a combination of Monte Carlo simulations and *exact* variational calculations. A key feature of our variational ansatz is that it allows for a variation in the connectedness of the domain and the shape of the domain boundary. Our main results are as follows. (i) In the achiral limit, optimum textures include virtual boojum, annular, and hedgehog phases. A novel feature is the occurrence of spontaneous chiral symmetry breaking to a chiral annular phase. (ii) When the domain shapes are allowed to deviate from circularity, then the tilt-induced anisotropic line tension typically gives rise to anisotropic domains whose shapes are roughly rectangular and elongated. (iii) A threshold chirality produces spiral defects and an unusual chiral tweed phase. (iv) Chirality induces large enough domains to break up into smaller domains, leading to a limiting domain size (keeping all other parameters fixed) and preventing coalescence.

In our theoretical study we have not included the effects of long-range multipolar (dipolar, quadrupolar) interactions; even so, we obtain a rich variety of shapes and shape transitions. In Ref. [36], we estimated the numerical values of parameters entering the Frank free energy, Eqs. (3) and (4), and showed that they are small compared to a typical dipolar interaction for the systems under consideration, providing a justification for dropping it. It is true, however, that a *long-range* dipolar interaction, if present, will always dominate at large length scales. In reality, dipolar interactions are screened; this introduces an additional length scale in the problem. If the screening length is large, then dipolar and quadrupolar interactions will crucially change the results reported here. This has been beautifully demonstrated in a series of experimental and theoretical studies on domains in lipid monolayers [40].

While our results are, in principle, applicable to a variety of systems featuring tilt domains of finite size embedded in a 2D substrate, our main interest is in the shapes and dynamics of domains in a multicomponent lipid mixture. GUVs composed of saturated and unsaturated lipid components typically exhibit a wide coexistence regime between a liquid disordered phase (enriched in the unsaturated component) and a gel phase (enriched in the saturated lipid), with the saturated lipid showing a tilt with respect to the plane of the membrane. Following a quench into this coexistence region, domains of the gel phase nucleate and grow in the liquid disordered phase. If the saturated lipid is chiral and/or if chiral impurities partition into the gel domain, then our analysis regarding the

shapes and dynamics of nucleating domains would hold. We look forward to experimental studies of these systems. We have recently studied an extension of this theory of orientational order on rigid membranes to the case of *active* polar filaments such as cortical actin on a rigid 2D surface [41].

ACKNOWLEDGMENTS

We thank Y. Hatwalne, N. V. Madhusudhana, and V. A. Raghunathan for useful discussions. M.R. acknowledges grants from CEFIPRA 3504-2 and HFSP.

[1] C. M. Knobler, Science **249**, 870 (1990).
[2] J. Korlach, P. Schwille, W. W. Webb, and G. W. Feigenson, Proc. Natl. Acad. Sci. USA **96**, 8461 (1999).
[3] C. Dietrich, L. A. Bagatolli, Z. N. Volovyk, N. L. Thompson, M. Levi, K. Jacobson, and E. Gratton, Biophys. J. **80**, 1417 (2001).
[4] A. V. Samsonov, I. Mihalyov, and F. S. Cohen, Biophys. J. **81**, 1486 (2001).
[5] L. A. Bagatolli and E. Gratton, Biophys. J. **77**, 2090 (1999).
[6] L. A. Bagatolli and E. Gratton, Biophys. J. **78**, 290 (2000).
[7] S. L. Veatch and S. L. Keller, Phys. Rev. Lett. **89**, 268101 (2002).
[8] S. L. Veatch and S. L. Keller, Biophys. J. **85**, 3074 (2003).
[9] T. Baumgart, S. T. Hess, and W. W. Webb, Nature **425**, 821 (2003).
[10] K. Simons and E. Ikonen, Nature **387**, 569 (1997).
[11] M. Edidin, Annu. Rev. Biophys. Biomol. Struct. **32**, 257 (2003).
[12] V. D. Gordon, P. A. Beales, Z. Zhao, C. Blake, F. C. MacKintosh, P. D. Olmsted, M. E. Cates, S. U. Egelhaaf, and W. C. K. Poon, J. Phys.: Condens. Matter **18**, L415 (2006).
[13] P. G. de Gennes and J. Prost, *The Physics of Liquid Crystals* (Clarendon Press, Oxford, UK, 1993).
[14] R. M. Weis and H. M. McConnell, Nature **310**, 47 (1984).
[15] J. Israelachvili, *Intermolecular and Surface Forces* (Academic Press, London, 1998).
[16] Th. Rasing, Y. R. Shen, M. W. Kim, and S. Grubb, Phys. Rev. Lett. **55**, 2903 (1985).
[17] K. Y. Lee and H. M. McConnell, Biophys. J. **68**, 1740 (1995).
[18] H. M. McConnell and V. T. Moy, J. Phys. Chem. **2**, 4520 (1988).
[19] J. Brewer, U. Bernchou, and L. A. Bagatolli, Biophys. J. **94**, 391 (2008).
[20] H. Mohwald, Annu. Rev. Phys. Chem. **41**, 441 (1990).
[21] C. M. Knobler and R. C. Desai, Annu. Rev. Phys. Chem. **43**, 207 (1992).
[22] A. Radhakrishnan and H. M. McConnell, Biochemistry **39**, 8119 (2000).
[23] S. Rivieŕe and J. Meunier, Phys. Rev. Lett. **74**, 2495 (1995).
[24] J. Fang, E. Teer, C. M. Knobler, K. K. Loh, and J. Rudnick, Phys. Rev. E **56**, 1859 (1997).
[25] S. A. Langer and J. P. Sethna, Phys. Rev. A **34**, 5035 (1986).
[26] S. A. Langer, R. E. Goldstein, and D. P. Jackson, Phys. Rev. A **46**, 4894 (1992).
[27] F. Xu and P. P. Crooker, Phys. Rev. E **56**, 6853 (1997).
[28] D. Pettey and T. C. Lubensky, Phys. Rev. E **59**, 1834 (1999).
[29] J. V. Selinger and D. R. Nelson, Phys. Rev. A **39**, 3135 (1989).
[30] J. V. Selinger and R. L. B. Selinger, Phys. Rev. E **51**, R860 (1995).
[31] P. C. Chaikin and T. C. Lubensky, *Principles of Condensed Matter Physics* (Cambridge University Press, Cambridge, 1995).
[32] J. P. Straley, Phys. Rev. A **14**, 1835 (1976).
[33] A. B. Harris, R. D. Kamien, and T. C. Lubensky, Rev. Mod. Phys. **71**, 1745 (1999).
[34] A. Yethiraj and A. van Blaaderen, Nature **421**, 513 (2003).
[35] R. C. Sarasij and M. Rao, Phys. Rev. Lett. **88**, 088101 (2002).
[36] R. C. Sarasij, S. Mayor, and M. Rao, Biophys. J. **92**, 3140 (2007).
[37] P. Galatola and J. B. Fournier, Phys. Rev. Lett. **75**, 3297 (1995).
[38] J. Rudnick and R. F. Bruinsma, Phys. Rev. Lett. **74**, 2491 (1995).
[39] B. R. Ratna, R. Shashidhar, G. G. Nair, S. K. Prasad, C. Bahr, and G. Heppke, Phys. Rev. A **37**, 1824 (1988).
[40] W. Ou-yang *et al.*, Thin Solid Films **516**, 2649 (2008); T. Yamamoto, T. Manaka, and M. Iwamoto, J. Chem. Phys. **126**, 125106 (2007).
[41] K. Gowrishankar and M. Rao, e-print arXiv:1201.3938v1, http://xxx.lanl.gov/.